Iranian Polymer Journal (2019) 28:881–893
https://doi.org/10.1007/s13726-019-00751-1

ORIGINAL RESEARCH

Chitosan/attapulgite/poly(acrylic acid) hydrogel prepared by glow-discharge electrolysis plasma as a reusable adsorbent for selective removal of Pb^{2+} ions

Jie Yu[1] · Quanfang Lu[1,2] · Jidong Zheng[1] · Yun Li[1]

Received: 13 May 2019 / Accepted: 14 September 2019 / Published online: 30 September 2019

Abstract
A chitosan/attapulgite/poly(acrylic acid) (CS/ATP/PAA) hydrogel was prepared by glow-discharge electrolysis plasma (GDEP) technique, in which *N*,*N'*-methylene-bis-acrylamide was acted as a crossing-linker, and then it was used as an adsorbent for the removal of Pb^{2+} ions from aqueous solutions. A possible polymerization mechanism is proposed. The structure, morphology and adsorption mechanism of CS/ATP/PAA hydrogel were characterized by FTIR, XRD, SEM and XPS techniques. The influences of pH, contact time and initial concentration on the Pb^{2+} adsorption were systematically examined. The selective adsorption of CS/ATP/PAA hydrogel for Pb^{2+} ions with the coexistence of Cd^{2+}, Co^{2+} and Ni^{2+} ions was investigated, as well. In addition, regeneration of hydrogel was also discussed in detail. The results indicated that the optimal adsorption pH was 4.8, and the time of adsorption equilibrium was 60 min. The adsorption behaviors fitted well to the pseudo-second-order kinetic model and Langmuir isotherm. The maximum adsorption capacity of CS/ATP/PAA hydrogel for Pb^{2+} ions based on Langmuir isotherm was 531.9 mg g^{-1}. The CS/ATP/PAA adsorbent exhibited promising selectivity for Pb^{2+} ions with the coexistence of Cd^{2+}, Co^{2+} and Ni^{2+} ions, and excellent reusability using EDTA-4Na solution as desorption solution. The adsorption process of Pb^{2+} ions on CS/ATP/PAA hydrogel was presented by the coordination between N or O atoms and Pb^{2+} ion, and the ion-exchange between Na^{+} and Pb^{2+} ions.

Keywords Chitosan · Hydrogel · Adsorption · Pb^{2+} ions · Selectivity · Reusability

Introduction

Water is the basis of all life in nature. However, with the development of chemical industry and extensive application of many chemical agents in agriculture, harmful compounds have been polluted air and soil, and consequently, drinking water, which resulted in numerous diseases [1, 2]. In these pollutants, heavy metal ions, such as Pb^{2+}, Cu^{2+}, Cd^{2+}, Ni^{2+}, Co^{2+} and Hg^{2+} ions, are prominent environmental issues which have become serious threats to ecological environment because heavy metals are not biodegradable and tend to accumulate in living tissues [3].

Lead ion (Pb^{2+}) is extensively found in nature but is considered as one of the most carcinogenic and hazardous elements [4]. Pb^{2+} ions in wastewater mainly come from battery industries, electronic manufacturing, mining, smelting, painting, and fertilizers [2, 4]. Long-term exposure to Pb^{2+} ions can be severely harmful to the urinary system, nervous system, immune system and blood system even at very low levels of Pb^{2+} intake, especially in children [5, 6]. Hence, the World Health Organization (WHO) has classified Pb^{2+} ion as a priority issue [7].

Various methods, for example, chemical precipitation, solvent extraction, ion-exchange, membrane separation and adsorption, have been developed for the removal of Pb^{2+} ions to satisfy the water pollution discharge standards [4, 6]. Among them, adsorption is considered as one of the outstanding methods because of its low cost, convenient operation, and simplicity in the post-treatment process [4,

✉ Jie Yu
yujie741008@163.com

✉ Quanfang Lu
luqf@nwnu.edu.cn

[1] College of Chemistry and Chemical Engineering, Northwest Normal University, Lanzhou 730070, China

[2] Editorial Department of the University Journal, Northwest Normal University, Lanzhou 730070, China

8]. Thus, in the long run, it is necessary to develop some adsorbents that are efficient, eco-friendly and sustainable.

Over the past 20 years, many materials, such as chitosan [9], lignin [10], clay [11] and zeolite [12] have been employed for the removal of Pb^{2+} ions. However, most of these materials show non-specificity for adsorption of Pb^{2+} ions because of their physical adsorption action. In addition, these adsorbents can easily become saturated with ubiquitous other ions, i.e., Mg^{2+}, Ca^{2+}, Na^{+} and K^{+} ions [5]. To improve the adsorption performance, seeking the novel adsorbent has been a research hotspot.

Recently, hydrogels as adsorbents have drawn a lot of attention for the removal of Pb^{2+} ions from wastewater due to their low cost, high adsorption capacity and fast adsorption rate [13, 14]. Owing to containing hydrophilic functional groups, e.g., –OH, –COOH, and $–NH_2$, most of the hydrogels can remove heavy metal ions through ion-exchange, complexation, electrostatic attraction and van der Waals forces [15].

However, many hydrogels used in practice are pure synthetic polymers. As is well-known, these hydrogels are toxic and non-biodegradable, therefore, they can cause serious environmental pollution. To overcome these flaws, development of environment-friendly composite hydrogels has aroused great interests.

Clays, such as montmorillonite [16], attapulgite [17, 18] and vermiculite [19] have been employed for the synthesis of novel organic/inorganic composites hydrogels. Attapulgite (ATP), a kind of hydrated octahedral-layered silicate mineral with reactive –OH groups, is easily grafted or dispersed into the matrix to form nanocomposites [17]. In addition, ATP is very abundant in nature and is much cheaper than other clays. Thus, in this work, ATP was selected as an excellent candidate for synthesizing organic/inorganic composites.

As the second most abundant polysaccharide in nature after cellulose, chitosan (CS) is low cost, non-toxic, biodegradable and biocompatible material. In addition, CS has abundant $–NH_2$ and –OH groups, which have strong chelation bonding with metal ions [20]. However, dissolubility in acidic media and poor adsorption capacity limit its industrial-scale application. To improve stability and increase adsorption property, it has been paid much attention to modification of CS [21, 22].

Many techniques have also been employed for the synthesis of hydrogels, such as chemical initiation [23], radiation [24], photo-curing [25] and glow-discharge electrolysis plasma (GDEP) [20]. Compared with other techniques, GDEP has simple steps and mild reaction conditions. In addition, GDEP can be acted as an environment-friendly technique because the reactive species such as HO· and H· are generated without requiring any additional chemicals. Moreover, HO· radicals produced by GDEP can be added into the polymer chains, therefore, the hydrogel possessed outstanding properties [14, 19].

Over the past 20 years, many studies for adsorption have focused on the kinetics, isotherms, and thermodynamics. Nevertheless, selectivity and regeneration of adsorbents were rarely studied. As is well-known, selective adsorption is very important for recovery some heavy metals from the mixture solution [8, 23]. The regeneration is another important factor for advanced adsorbents. Those adsorbents that have better reusability features will markedly reduce the overall cost.

In general, acids possess higher desorption capacities than bases, inorganic salts and water [8, 15]. However, the concentration of acid is so high (about pH=1) that will corrode equipment during the desorption process. Therefore, finding new eluent is of great interest.

In this study, a novel organic/inorganic composites hydrogels, that is, chitosan/attapulgite/poly(acrylic acid) (CS/ATP/PAA) was prepared using a simple one-step method by glow-discharge electrolysis plasma (GDEP) technique, in which *N*,*N*'-methylene-bis-acrylamide was used as a crossing-linker. A possible polymerization mechanism induced by GDEP is proposed. The structure and morphology were characterized by FT-IR, XRD and SEM techniques. The influences of pH, contact time and initial concentration on the adsorption of Pb^{2+} ions were examined. The kinetic for selective adsorption of CS/ATP/PAA toward Pb^{2+} ions with the coexistence of other ions, i.e., Cd^{2+}, Co^{2+} and Ni^{2+} was investigated. Desorption and regeneration of hydrogel in HNO_3 and ethylenediaminetetraacetic acid tetrasodium salt (EDTA-4Na) as eluent were discussed, respectively. Moreover, based on the XPS analysis, the adsorption mechanism was also elucidated.

Experimental

Materials

Chitosan (CS, deacetylation degree > 85%) was supplied by Zhejiang Golden-Shell Biochemical Co., Zhejiang, China. Attapulgite (ATP) was attained from Jiuchuan Nano-Material Technology Co., Ltd., Jiangsu, China. Acrylic acid (AA, analytical grade) was purchased from Tianjin Guangfu Chemical Research Institute, Tianjin, China, and then distilled under reduced pressure before use. *N*,*N*′-methylene-bis-acrylamide (MBA, chemical pure) was obtained from Shanghai Chemical Reagent Corporation, Shanghai, China. HNO_3, NaOH, $Pb(NO_3)_2$, $Ni(NO_3)_2{\cdot}6H_2O$, $Co(NO_3)_2{\cdot}6H_2O$, $Cd(NO_3)_2{\cdot}4H_2O$ and ethylenediaminetetraacetic acid tetrasodium salt (EDTA-4Na) were analytical reagent and received from Shanghai Chemical Reagent Co., Shanghai, China.

Preparation of CS/ATP/PAA absorbent

The details of the experimental device have been described in previous work [26]. Typically, 0.5 g CS and 0.3 g ATP were added into a three-neck flask with 55 mL distilled water. To disperse evenly, the mixture was stirred with 120 r min^{-1} at 75 °C for 20 min. Then, 10 mL AA and 0.2 g MBA were added into the mixed solution for 10 min to dissolve CS and MBA, completely. After that, two electrodes were inserted into the mixed solution to start the glow discharge for 10 min at 650 V and 82 mA.

After the discharge, the mixed solution was stirred for another 4 h at 75 °C. And then, the product was cooled to 25 °C, cut into small pieces about 2-5 mm, and neutralized the carboxylic groups of the grafted poly(acrylic acid) by NaOH solution to a degree of neutralization for about 80%. Finally, the resulting product was washed several times with ethanol, dried in freeze-drying oven and milled through a 150 μm sieve. The yield (gel content) of the CS/ATP/PAA was about 53%.

Characterization of CS/ATP/PAA hydrogel

The optical emission spectra of GDEP at 200–800 nm were determined by an AvaSpec-2048-8 optical fiber spectrometer (Netherlands). Fourier transform infrared spectra (FTIR) of CS/ATP/PAA were recorded on a DIGILAB FTS 3000 FTIR spectrophotometer (USA). X-ray diffraction (XRD) patterns were carried out by a Rigaku D/max-2400 X-ray power diffractometer (Japan). Surface morphology of CS/ATP/PAA was observed on a Zeiss Ultra plus field emission scanning electron microscope (FESEM, Germany). X-ray photoelectron spectroscopy (XPS) of CS/ATP/PAA before and after adsorption of Pb^{2+} was carried out on a PHI-5702 X-ray photoelectron spectrometer (USA). The concentrations of heavy metal ions were determined by Varian 715-ES ICP-AES (Varian, USA). All pH measurements were performed with a pHS-3C (INESA, China).

Adsorption studies

Influence of pH

The solution pH ranged from 1.0 to 5.9 was adjusted with 0.1 mol L^{-1} HNO_3. Amounts of 0.03 g CS/ATP/PAA and 100 mL heavy metal ions solution (1.5 mmol L^{-1}) were added into a conical flask. Then, the mixtures were shaken at 140 r min^{-1} for 3 h. The adsorption capacity [8] was calculated as follows:

$$Q_t = \frac{(C_0 - C_t)V}{m} \quad (1)$$

where Q_t (mg g^{-1}) is the adsorption capacity at any time t (min), m (g) is the quality of CS/ATP/PAA, C_0 and C_t (mg L^{-1}) are the concentrations of the heavy metal ions at initial and any time t, and V (L) is the volume of the solution.

Selective adsorption

To investigate the selectivity of CS/ATP/PAA adsorbent, 0.06 g CS/ATP/PAA was added into 200 mL mixture solution containing Pb^{2+}, Cd^{2+}, Co^{2+} and Ni^{2+} ions (each concentration of 1.5 mmol L^{-1}). Then, the concentrations of metal ions were determined by ICP-AES at certain intervals. The adsorption capacities were calculated by Eq. (1). The distribution coefficients K_d (L g^{-1}) is defined as follows [8, 27]:

$$K_d = \frac{C_0 - C_e}{C_e} \times \frac{V}{m} \quad (2)$$

where C_0 and C_e (mg L^{-1}) are the concentrations of metal ions before and after adsorption, respectively, V (L) is the volume of solution, and m (g) is the mass of adsorbent. Then, the selectivity coefficient α is calculated as follows [27]:

$$\alpha = \frac{K_d(Pb^{2+})}{K_d(\text{Competition ion})} \quad (3)$$

where K_d (Pb^{2+}) and K_d (Competition ion) are the distribution coefficients of Pb^{2+} ion and competition ion, i.e., Cd^{2+}, Co^{2+} and Ni^{2+}, respectively.

Adsorption kinetics and adsorption isotherm

An amount of 0.06 g CS/ATP/PAA adsorbent was added into 200 mL Pb^{2+} solution (1.5 mmol L^{-1}, pH = 4.8) and shaken at 140 r min^{-1}. Then, the solutions were taken at a specified time intervals and the concentration of Pb^{2+} ions was determined by ICP-AES. The adsorption capacity of Pb^{2+} was calculated by using Eq. (1).

Into a series of the 100 mL solutions with different initial concentration of Pb^{2+} (pH = 4.8), 0.03 g CS/ATP/PAA was added and shaken at 140 r min^{-1} for 3 h. The concentration of Pb^{2+} ions was determined and the adsorption capacities were calculated by Eq. (1).

Desorption and reusability

To find an effective method for desorption of adsorbed Pb^{2+} ions, two different eluents (0.5 mol L^{-1} HNO_3 and 1.5 mmol L^{-1} EDTA-4Na solution) were used. Into a series of the 100 mL of solutions of Pb^{2+} ions (1.5 mmol L^{-1}, pH = 4.8), 0.03 g adsorbent was added and shaken at 140 r min^{-1} for 3 h. Then, the concentration of solutions was determined using

ICP-AES and the adsorption capacities were calculated by Eq. (1). After that, CS/ATP/PAA adsorbents with absorbed Pb^{2+} ions were removed and placed into two different eluents and shaken at 140 r min^{-1}. To study the reusability, sequential adsorption-desorption experimental was repeated 4 times.

Results and discussion

Preparation mechanism of CS/ATP/PAA

An emission spectrum between 200 and 800 nm for GDEP in mixture solution of AA and CS at 650 V discharge voltage is presented in Fig. 1. The bands at 262.0, 283.0 and 306.0–309.0 nm are assigned to the lines of OH ($A^2\Sigma^+ \rightarrow X^2\Pi$). Because lots of water is vaporized during discharge, electrons collide with the H_2O molecules to produce OH^+, which impact with electrons to form OH [28].

A series of O II lines spread from 391.2 to 470.1 nm are produced from water vapor by electron impact [29]. The strongest emission lines at 486.1 and 656.3 nm are attributed to the H_β and H_α, stemming from electrolyte around the cathode which is bombarded by electrons [28, 30]. The emission line of O I is also observed at 777.1 nm [28].

In addition, the spectral line of Na I is also appeared at 589.0 and 589.6 nm, this suggested that the solutions contain a small amount of Na^+. All above information indicated that GDEP can produce various reactive radicals (HO·, H·, O·, etc.), among which HO· is one of the strongest oxidants ($E^0_{HO/H_2O} = 2.85$ V) [28]. Therefore, HO· radicals play the most important role in inducing chemical reactions by GDEP [31, 32].

Generally speaking, in addition to the hydrogen abstraction on labile H of hydrocarbon chains (HO + RH $\rightarrow H_2O$ + R·), HO· can also take part in electrophilic addition to unsaturated bond [33] as follows:

$$HO + R_2C = CR_2 \rightarrow R_2(OH)C - CR_2$$

Thus, during the induced copolymerization of CS, ATP and AA by GDEP, the reactions of hydrogen abstraction from CS and ATP, and electrophilic addition of AA are coexisted. A possible mechanism for the preparation of CS/ATP/PAA copolymer by GDEP is illustrated in Scheme 1. First, H_2O molecules are dissociated into HO·, H· and O· radicals by high-energy electrons from GDEP, which is called the radicals forming process (reaction 1).

Then, HO· radicals react with labile H from ATP and CS by the abstraction of hydrogen to form the new radicals (a, b and c moieties in reaction 2). Meanwhile, HO· radicals also add to the unsaturated double C=C bonds of AA forming the new organic radicals (d moiety in reaction 2). The above reactions are called the chain initiation process (reaction 2). After that, these radicals (a, b, c and d) randomly react with AA to form macromolecule free radicals (e, f, g and h moieties in reaction 3) and cause the chain propagation (reaction 3).

Finally, reactions of macromolecule radicals are terminated by cross-linking copolymerization of MBA, radical-radical combinations and disproportionations to form a three-dimensional network copolymer, which is called the termination reaction (reaction 4) [8, 13, 26]. And then, the -COOH groups of the grafted poly(acrylic acid) were neutralized and the resulting product was obtained (reaction 5).

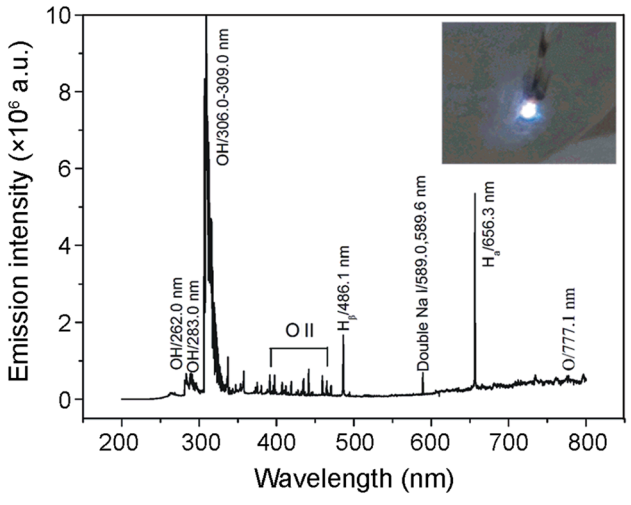

Fig. 1 Emission spectrum of the GDEP in mixed solution of AA and CS at 650 V discharge voltage (inset is the photograph of discharge at 650 V)

Characterization of CS/ATP/PAA

Figure 2a shows the FTIR spectra of CS, ATP, AA and CS/ATP/PAA. The peaks of CS are at 3435 cm^{-1} (N–H and O–H), 1599 cm^{-1} (NH_2 bend), 1157 cm^{-1} (C–O–C, glucosidic bond), 1030 cm^{-1} (C6–OH) and 1082 cm^{-1} (C3–OH) [8]. The peaks of ATP are at 3621 cm^{-1} (O–H stretch of Mg–OH unite) [34], 3549 cm^{-1} (O–H stretch of Al–OH unite), 3419 cm^{-1} (O–H stretch of adsorbed water and zeolitic water) [35], 1027 cm^{-1} (Si–O–Si stretch) and 777 cm^{-1} (Si–O–Mg stretch). The peaks of AA are at 1631 cm^{-1} (C=C stretch) and 1711 cm^{-1} (C=O stretch) [20]. When the CS/ATP/PAA was formed, the peaks at 1599 cm^{-1} (–NH_2 bend) of CS, 3621 (O–H stretch of Mg–OH) and 3549 cm^{-1} (O–H stretch of Al–OH) of ATP, and 1631 cm^{-1} (C=C stretch) of AA have been disappeared nearly. Meanwhile, new peaks at 1559 (C=O of $–COO^-$ asymmetric stretch) [36] and 794 cm^{-1} (Si–O–Mg stretch) have appeared. All above

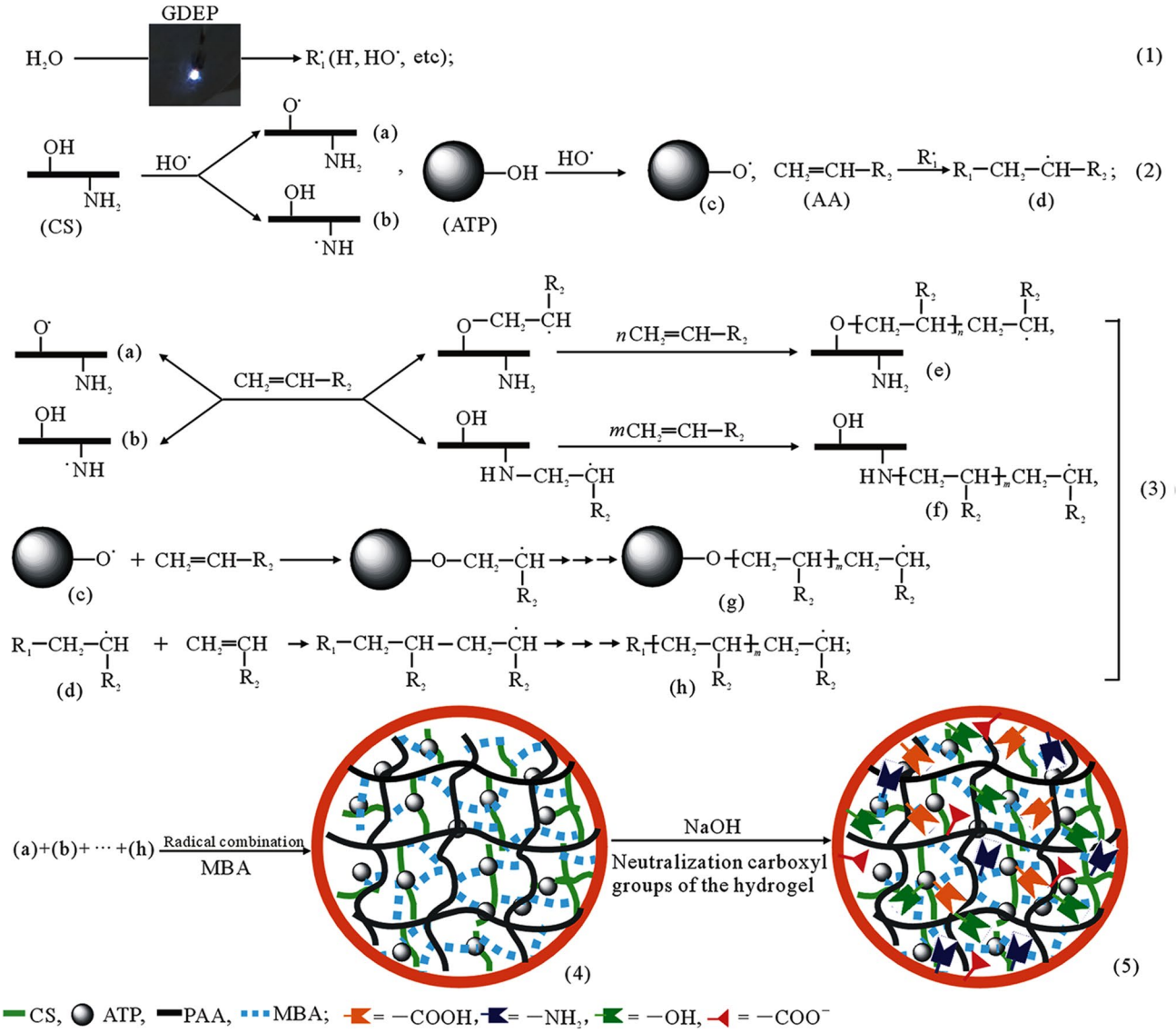

Scheme 1 Proposed polymerization mechanism of CS/ATP/PAA hydrogels induced by GDEP. (1) radical formation, (2) chain initiation, (3) chain propagation, (4) chain termination, and (5) neutralization carboxyl groups of the poly(acrylic acid)

information indicated that CS/ATP/PAA has been successfully synthesized by GDEP technique.

Figure 2b shows the XRD patterns of CS, ATP and CS/ATP/PAA. It can be seen that CS shows two strong diffraction peaks at $2\theta = 11.91°$ and 20.18°, respectively. This shows that strong intermolecular and intramolecular hydrogen bonds in CS formed crystalline regions [20]. A typical (110) diffraction peak of ATP appears at $2\theta = 8.16°$. In addition, the peaks at $2\theta = 19.61°$, 20.48°, 26.44°, 27.02° and 34.98° are attributed to quartz and dolomite impurities of ATP [14].

However, after graft copolymerization with CS, ATP and AA, the whole peak intensity of CS/ATP/PAA decreased sharply and the peak shape widened. This shows that the graft polymerization formed an amorphous composite [20]. In addition, the peaks at 11.91° and 20.18° of CS were disappeared, which indicated that the graft copolymerization changed the crystallinity of CS and the structure of copolymer became very disorder. Moreover, after graft copolymerization, the typical diffraction peaks of ATP maintained almost no change, i.e., the peaks of ATP were at 7.98°, 19.78°, 20.82°, 26.64°, 27.22° and 35.12° in the CS/ATP/PAA copolymer, indicating that the interactions of CS and AA during polymerization only occur on the surface of the ATP without destroying the original crystallinity of the ATP [14].

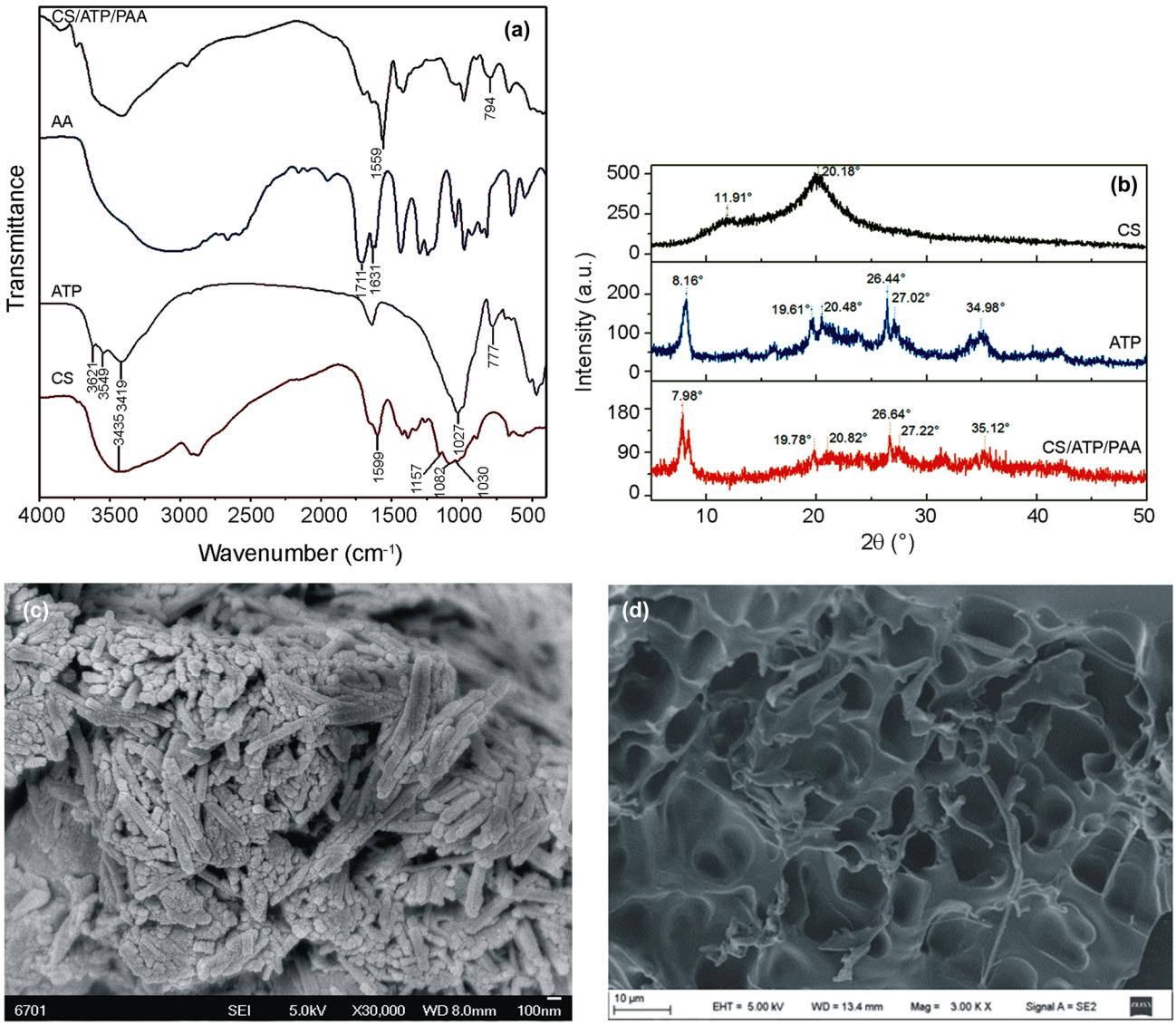

Fig. 2 FTIR spectra of CS, ATP, AA and CS/ATP/PAA (**a**); XRD patterns of CS, ATP and CS/ATP/PAA (**b**) samples, and SEM micrographs of ATP (**c**) and CS/ATP/PAA hydrogel (**d**)

The surface morphology of ATP and CS/ATP/PAA is shown in Fig. 2c, d, respectively. As can be seen from Fig. 2c, the ATP presents unique rod-like structure [14]. The length of the nanorods is about 400–800 nm. After graft copolymerization of ATP with CS and AA, the surface of CS/ATP/PAA hydrogel (Fig. 2d) has three-dimensional network structure with many pores. In addition, the ATP nano-particle was dispersed well in CS/ATP/PAA matrix, and the interface between the CS, PAA and ATP is not very clear. This means that AA was grafted onto the CS and ATP backbone to form a porous copolymer. The rough surface and porous structure can increase the area of contact with the solution, facilitate heavy metal ions to diffuse into the network structure, accelerate the adsorption rate and improve the adsorption capacity [8, 13, 20].

Adsorption performance

Influence of pH on the adsorption

The solution pH is an important parameter because it not only affects the existing form of the heavy metal ions in solution but also influences the protonation and surface charge of the functional groups on the hydrogel [37, 38]. Due to the

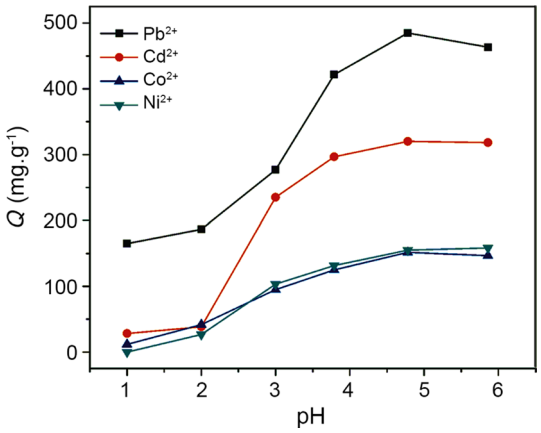

Fig. 3 Variation of the adsorption of heavy metal ions vs. pH

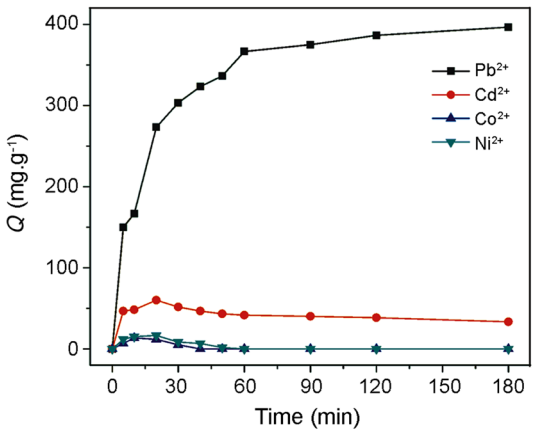

Fig. 4 Selective adsorptions of Pb^{2+}, Cd^{2+}, Co^{2+} and Ni^{2+} ions in a mixed solution of 1.5 mmol L^{-1} of these ions at pH = 4.8

forming of metal hydroxide precipitates at neutral or alkaline environment, the pH range from 1.0 to 5.9 was examined.

Figure 3 reveals the influence of solution pH on the adsorption capacity of Pb^{2+}, Cd^{2+}, Co^{2+} and Ni^{2+} ions by CS/ATP/PAA adsorbent. It is obvious that the adsorption capacity of the metal ions increased with increasing the solution pH and the optimal adsorption was achieved at pH = 4.8. At lower pH, hydrogen ions have strong competition with metal ions for the available sites [39, 40]. Meanwhile, the amino and carboxyl groups are readily protonated to prevent the chelation interaction between these groups and heavy metals. With the increase of the solution pH, the numbers of H^+ ions decreased and the competition was weakened [8, 41] and the protonation degrees of amino and carboxyl groups were reduced. Thus, the adsorption capacities of metal ions were increased.

Selective adsorption

To estimate the selectivity of CS/ATP/PAA adsorbent for metal ions, adsorption experiment was implemented with mixed solutions containing 1.5 mmol L^{-1} Pb^{2+}, Cd^{2+}, Co^{2+} and Ni^{2+} ions at pH = 4.8.

Figure 4 illustrates the adsorption capacity at different contact time. As can be seen from Fig. 4, the adsorption capacity of Pb^{2+} gradually increased as the contact time increased, however, the adsorption capacities of the other heavy-metal ions increased at early 20 min, then gradually declined, and finally become almost negligible for Co^{2+} and Ni^{2+} ions after 3 h. Clearly, the initially adsorbed Cd^{2+}, Co^{2+} and Ni^{2+} ions on the adsorbent were gradually replaced by Pb^{2+}ions, and subsequently released into the solution through a competitive adsorption process [8]. It indicated that the coordination bond between Pb^{2+} ions and chelating groups (–OH, –COOH, and $–NH_2$) was more stable than the other heavy-metal ions (i.e., Cd^{2+}, Co^{2+} and Ni^{2+}) and the CS/ATP/PAA adsorbent showed promising selectivity for Pb^{2+} after 3 h.

The distribution coefficient (K_d) and selectivity coefficient (α) are often used to evaluate the selectivity of an adsorbent. Higher values of K_d suggested that the metal ions were maintained in the solid phase, while low values of K_d indicated that a large fraction of the metal ions remained in the solution. The greater the value of α is, the better will be the selectivity [42]. The calculated values of K_d and α of adsorbed metal ions on CS/ATP/PAA adsorbent are listed in Table 1.

As shown in Table 1, the K_d value of Pb^{2+} ion was higher than that of the other heavy-metal ions. Moreover, the value of α for Pb^{2+} ion was greater, as well. It further indicated that the CS/ATP/PAA copolymer has excellent selectivity for adsorption of Pb^{2+} ions in coexistence with Cd^{2+}, Co^{2+} and Ni^{2+}ions.

Influence of contact time on Pb^{2+} adsorption

Figure 5 shows the adsorption capacity of Pb^{2+} on CS/ATP/PAA adsorbent with contact time at 25 °C. As shown in Fig. 5, plot a, the adsorption capacity increased rapidly in initial 5 min. This fast absorption rate can be assigned to plenty of

Table 1 The Q_e, K_d and α values for Pb^{2+}, Cd^{2+}, Co^{2+} and Ni^{2+} ions on CS/ATP/PAA adsorbent

Metal ions	Q_e		K_d, L g^{-1}	α (Pb^{2+}/B^{2+})
	mg g^{-1}	mmol g^{-1}		
Pb^{2+}	396.7	1.915	2.093	–
Cd^{2+}	33.33	0.297	0.208	10.06
Co^{2+}	0	0	0	∞
Ni^{2+}	0	0	0	∞

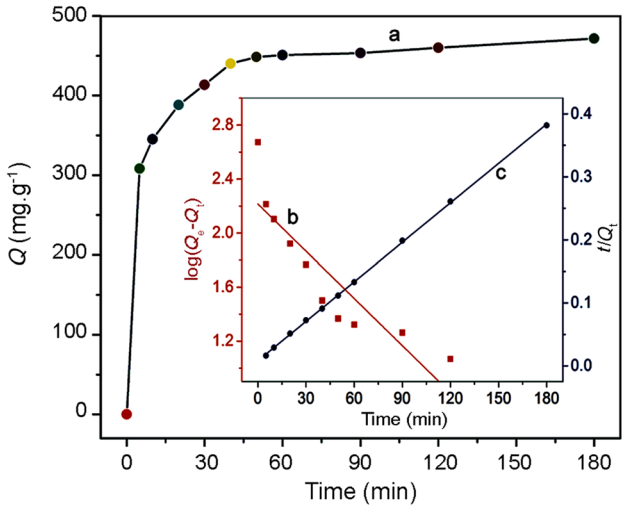

Fig. 5 Adsorption kinetics (**a**), pseudo-first-order kinetics model (**b**) and pseudo- second-order kinetics model (**c**) of Pb^{2+} ions on CS/ATP/PAA hydrogel

available active sites on the CS/ATP/PAA. Then, the adsorption capacity increased slowly from 5 to 50 min. As the adsorption continued, the active sites were decreased, the adsorption rates slowed down [43], and Pb^{2+} ions diffused into the network structure. After 60 min, the available sites were all occupied and the adsorption capacity tends to remain the same achieving the adsorption equilibrium. The equilibrium adsorption capacity of Pb^{2+} ion was 471.7 mg g^{-1} at 60 min; suggesting that CS/ATP/PAA copolymer had rapid adsorption rate and high adsorption capacity.

To investigate the potential rate-controlling step and adsorption mechanisms for removal of Pb^{2+}ions, two kinetic models, i.e., the pseudo-first-order model and pseudo-second-order model were used for analyzing the experimental data. The linear forms of two equations are given as follows:

$$\text{Pseudo-first-order model}: \log\left(Q_e - Q_t\right) = \log Q_e - \frac{k_1}{2.303}t \quad (4)$$

$$\text{Pseudo-second-order model}: \frac{t}{Q_t} = \frac{1}{k_2 Q_e^2} + \frac{t}{Q_e} \quad (5)$$

where Q_e and Q_t (mg g^{-1}) are the adsorption capacities at equilibrium and at certain time t (min), respectively. k_1 (min^{-1}) and k_2 (g mg^{-1} min^{-1}) are the rate constants of the pseudo-first-order and pseudo-second-order, respectively.

The fitting of experimental data with the two adsorption kinetic models is presented in inset figure in Fig. 5, plots b and c. As shown in Fig 5, the experimental data of pseudo-second-order model are fitted better than that of the pseudo-first-order model. The kinetic parameters are presented in Table 2. Compared with the parameters of the two models for Pb^{2+} adsorption, it was found that the R^2 (0.9997) value of the pseudo-second-order model was closer to unity 1 and the Q_e values ([Pb^{2+}]= 478.5 mg g^{-1}) of the pseudo-second-order model was closer to the experimental $Q_{e,exp}$ value ([Pb^{2+}]= 471.7 mg g^{-1}). This indicated that the rate-limiting step of Pb^{2+} adsorption on CS/ATP/PAA is a chemisorption process [44].

Influence of initial concentration

The adsorption capacities of CS/ATP/PAA adsorbent for Pb^{2+} ions at initial and equilibrium concentrations are presented in Fig. 6, plots a and b, respectively. Obviously, the adsorption capacities increased with increasing the initial and equilibrium concentrations of Pb^{2+} ions. This is because the higher the Pb^{2+} ions concentration, the more active adsorption sites of CS/ATP/PAA were involved [10]. When the active adsorption sites were all occupied, the adsorption capacities were slowly increased to a saturated value. The experimental saturated adsorption capacity of Pb^{2+} ions on CS/ATP/PAA was 523.3 mg g^{-1}. This suggested that CS/

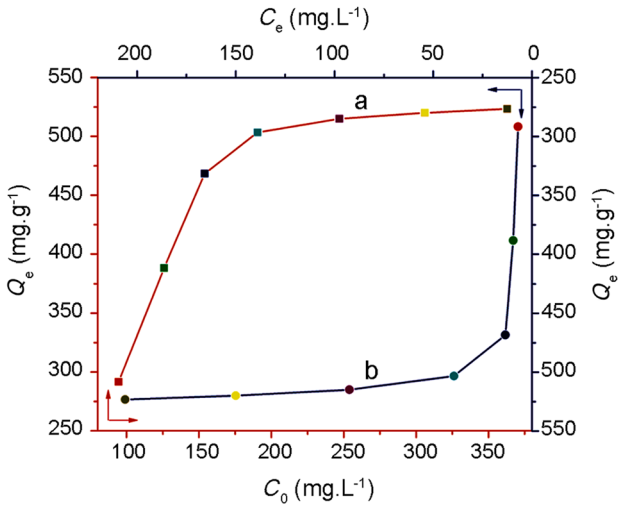

Fig. 6 The effect of initial concentration (**a**) and equilibrium concentration (**b**) on Pb^{2+} adsorption of CS/ATP/PAA hydrogel

Table 2 Kinetic parameters of Pb^{2+} ions adsorption on CS/ATP/PAA hydrogel

$Q_{e,exp}$, mg g^{-1}	Pseudo-first-order model			Pseudo-second-order model		
	$k_1 \times 10^{-2}$, min^{-1}	q_e, mg g^{-1}	R^2	$k_2 \times 10^{-4}$, g mg^{-1} min^{-1}	q_e, mg g^{-1}	R^2
471.7	2.68	163.9	0.7716	5.23	478.5	0.9997

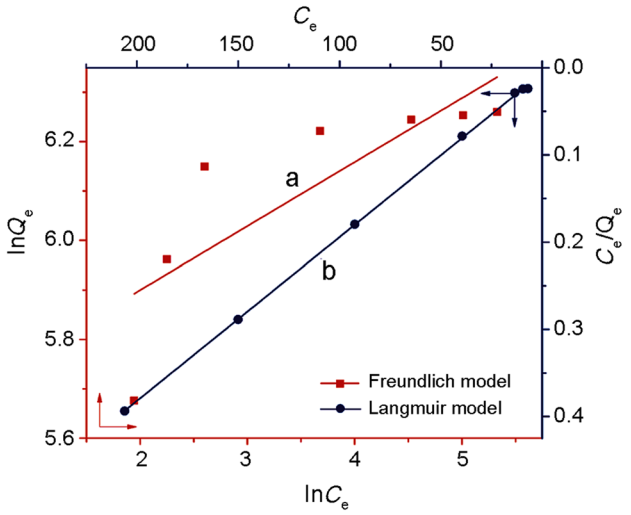

Fig. 7 Freundlich (**a**) and Langmuir (**b**) isotherm models of Pb^{2+} ions adsorption on CS/ATP/PAA hydrogel at pH = 4.8 and 25 °C

ATP/PAA adsorbent has higher adsorption capacity for Pb^{2+} ions.

To further investigate the adsorption mechanism of Pb^{2+} ions on CS/ATP/PAA, both Freundlich and Langmuir isotherm models were employed for analyzing the experimental data. The linear forms of the two isotherm equations are described as follow:

$$\text{Freundlich}: \ln Q_e = \ln K_F + \frac{1}{n} \ln C_e, \tag{6}$$

$$\text{Langmuir}: \frac{C_e}{Q_e} = \frac{1}{K_L Q_m} + \frac{C_e}{Q_m} \tag{7}$$

where C_e (mg L^{-1}) is the equilibrium concentration of Pb^{2+} ion, K_F (Lg^{-1}) is the Freundlich constant related to the adsorption capacity, n is another constant related to adsorption intensity, Q_m (mg g^{-1}) is the maximum adsorption capacity, and K_L (L mg^{-1}) is the Langmuir constant related to the energy of adsorption.

As shown in Fig. 7, the Langmuir isotherm agrees with the experimental data better than the Freundlich model. The isotherm parameters are listed in Table 3. Compared with Freundlich isotherm model, the R^2 of Langmuir isotherm model was closer to 1. In addition, the maximum adsorption capacity (Q_m) ([Pb^{2+}]= 523.3 mg g^{-1}) from Langmuir model are closer to the experimental $Q_{e,exp}$ value ([Pb^{2+}]= 531.9 mg g^{-1}). The results suggested that the adsorption process of Pb^{2+} ions on CS/ATP/PAA is a monolayer chemisorption.

Many works have reported the removal of Pb^{2+} ions by modified chitosan or clay from aqueous solutions. To evaluate the adsorption performance of CS/ATP/PAA hydrogel synthesized by GEDP technique, its maximum adsorption capacity was compared with other materials, which were obtained by other techniques and listed in Table 4. As shown in Table 4, unmodified lignin, chitosan, attapulgite, and natural zeolite were all showed lower adsorption. Instead, modified composite materials had higher adsorption capacity. Moreover, the CS/ATP/PAA adsorbent had the highest adsorption capacity, indicating that GEDP technique can be considered as an alternative promising method for the preparation of organic/inorganic composite materials with high adsorption performance.

Table 3 Isotherms parameters for Pb^{2+} adsorption on CS/ATP/PAA hydrogel

$Q_{e,exp}$, mg g^{-1}	Freundlich model			Langmuir model		
	K_F, L mg^{-1}	n	R^2	K_L, L mg^{-1}	Q_m, mg g^{-1}	R^2
523.3	281.6	7.72	0.6018	0.295	531.9	0.9997

Table 4 Comparison of adsorption capacities of Pb^{2+} ions on CS/ATP/PAA hydrogel and other adsorbents

Adsorbent	Preparing method	Q (mg g^{-1})	References
CS/ATP/PAA hydrogel	GDEP technique	523.3	This work
Xanthate-modified thiourea chitosan sponge	Chemical modification	188.04	[4]
CS/PEG/PAA hydrogel	GDEP technique	431.7	[8]
Chitosan	Crab shells	78.74	[9]
Lignin	Precipitation from black liquor	14.30	[10]
Palygorskite	–	20.72	[11]
Natural zeolite	–	20.72	[12]
ATP/PAA microgel	Ammonium persulfate initiation	196.5	[17]
EMATP	Chemical modification	258.0	[18]
PEO/CS membrane	Electrospinning	214.8	[22]
PAACS adsorbent	Grafted and cross-linked	734.3	[23]
Chitosan functionalized with xanthate flakes	Chemical modification	322.6	[44]

Desorption and reusability

Figure 8 presents the reuse potential of the CS/ATP/PAA adsorbent by 4 times sequential adsorption-desorption cycle using 0.5 mol L^{-1} HNO_3 and 0.015 mol L^{-1} EDTA-4Na solutions as eluents. As can be seen from Fig. 8, CS/ATP/PAA absorbent showed a good reusability in EDTA-4Na solution. Compared with the first adsorption capacity, the second adsorption capacity falls 52.6% using HNO_3 solution as eluent. This is because most of carboxy groups (–COOH) of CS/ATP/PAA have been converted into –COONa after neutralized to a degree for about 80%. The Na^+ ions were exchanged with the Pb^{2+} ions in the adsorption process [45]. In addition, the adsorbed Pb^{2+} ions were exchanged with H^+, and accordingly, the active groups such as $–COO^-$ were protonated to form –COOH which suppressed the chelation interaction between Pb^{2+} ions and these active groups due to hydrogen-bond interaction. Moreover, chelated Pb^{2+} ions on CS/ATP/PAA absorbent were not desorbed completely in HNO_3 solution. Therefore, the second adsorption capacity of CS/ATP/PAA absorbent was lower than that of the first. However, the second adsorption capacity using EDTA-4Na solution as eluent rose 22.7% compared with the first adsorption capacity. This is because the adsorbed Pb^{2+} ions are exchanged with Na^+ after desorption in EDTA-4Na solution. Meanwhile, part of unneutralized –COOH was deprotonated. What's more, chelated Pb^{2+} ions on CS/ATP/PAA absorbent were desorbed completely in EDTA-4Na solution because EDTA-4Na has stronger chelating property than that of CS/ATP/PAA copolymer [15]. All the above facts indicated that the CS/ATP/PAA absorbent has a good reusability using EDTA-4Na solutions as eluent and can recover Pb^{2+} ions from aqueous solutions.

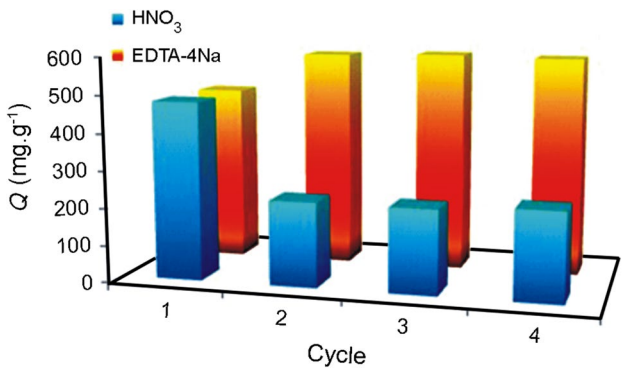

Fig. 8 Adsorption capacities of Pb^{2+} ions at sequential 4 adsorption-desorption cycles using 0.5 mol L^{-1} HNO_3 and 0.015 mol L^{-1} EDTA-4Na as eluents

Adsorption mechanism

XPS is extensively used to distinguish the different forms of the same element and identify the existence of a particular element in a material [4, 46]. Electron-donating ligands decrease the binding energy (BE) of the core level electrons, while electron-withdrawing ligands raise their BE [15, 47]. Figure 9a illustrates the full XPS spectra of CS/ATP/PAA copolymer before and after adsorption of Pb^{2+} ions.

Obviously, the peaks of Na 2p (32.3 eV), Na 2s (64.0 eV), Na (A) (498.0 eV) and Na 1s (1075.0 eV) in CS/ATP/PAA copolymer almost completely disappear after adsorption of Pb^{2+} ions. The new peaks, such as Pb 5d (22.5 eV), Pb 4f (143.2 eV), Pb 4d (414.4, 436.4 eV) and Pb 4p (646.0 eV) were appeared after adsorption of Pb^{2+} ions. It indicated that Na^+ ions were displaced by Pb^{2+} ions during the adsorption process. This revealed that ion-exchange may play an important role in Pb^{2+} adsorption process [13, 15].

Figure 9b, c shows the high-resolution XPS spectra of the N 1s and O 1s before and after adsorption of Pb^{2+} ions. It is noticeable that the binding energies of N 1s (BE = 399.3 eV) and O 1s (BE = 531.4 eV) were shifted to higher binding energy (399.7 eV and 531.6 eV) after the adsorption. This is because complexation was formed through a coordinated covalent bond [47], in which a lone pair of electrons in O and N atom were donated to the shared bond between N or O atoms and Pb^{2+} ions [8, 48]. Therefore, the electron cloud densities of the N and O are reduced, and thus a higher binding energy was observed [49].

Figure 9d shows the XPS spectrum of the Pb 4f in CS/ATP/PAA adsorbent after adsorption of Pb^{2+} ions. As shown in Fig. 9d, deconvolution of Pb 4f spectrum showed four separated peaks. The peaks at 143.5 and 138.6 eV are assigned to the typical Pb $4f_{5/2}$ and Pb $4f_{7/2}$ of Pb^{2+} ions. The other two at 141.5 and 136.6 eV are identified from Pb^{2+} complexation [50]. The above phenomenon means that Pb^{2+} complexation was formed. Based on the competitive adsorption, reusability and XPS analysis, proposed selective adsorption and desorption mechanism between the CS/ATP/PAA hydrogel and Pb^{2+} ions are shown in Scheme 2.

Conclusion

A functional chitosan/attapulgite/poly(acrylic acid) (CS/ATP/PAA) hydrogel has been synthesized by GDEP technique. FTIR, XRD and SEM analysis indicated that CS/

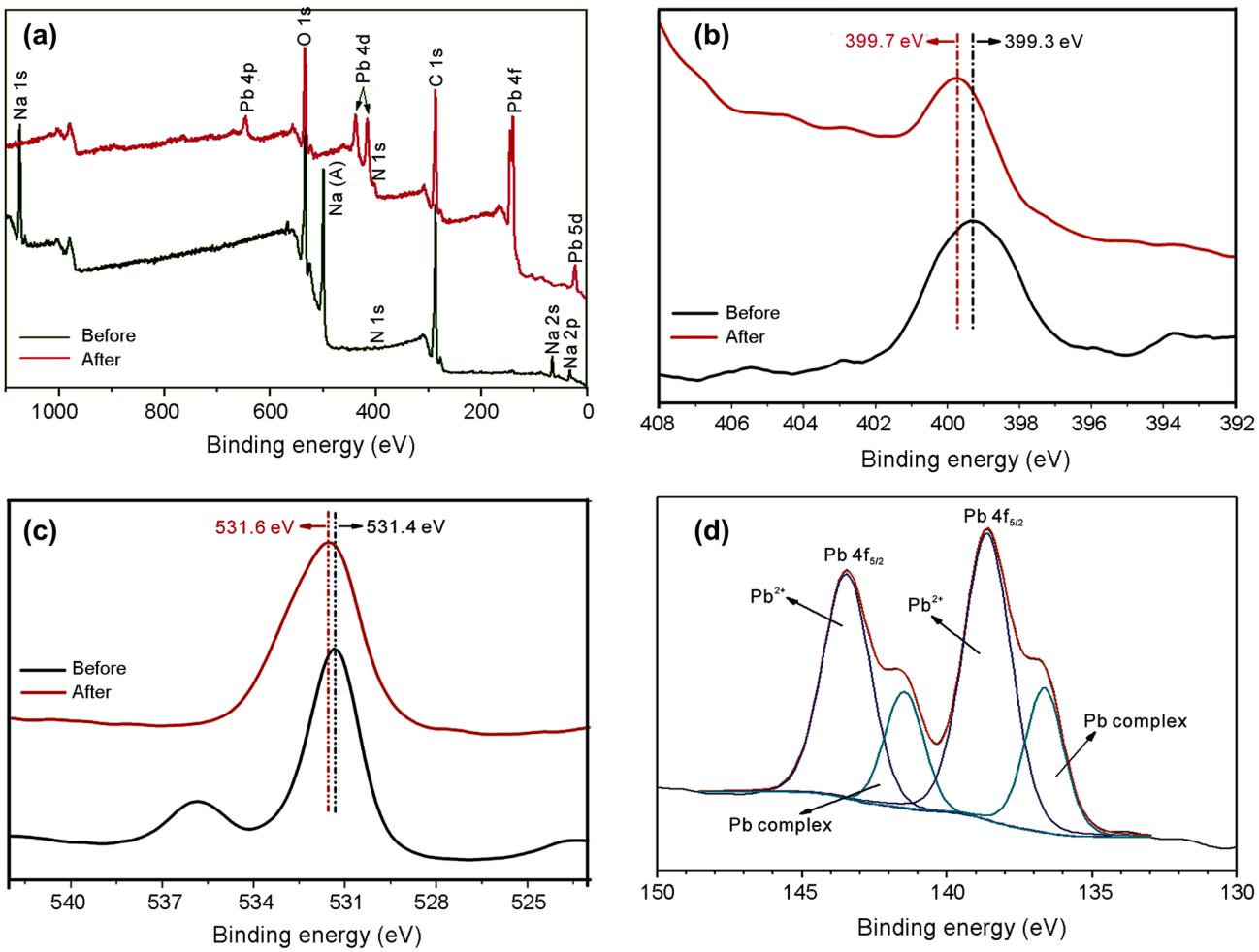

Fig. 9 XPS spectra of CS/ATP/PAA adsorbent before and after adsorption of Pb^{2+}: **a** full spectra, **b** N 1s spectra, **c** O 1s spectra, and **d** Pb 4f spectra in CS/ATP/PAA adsorbent

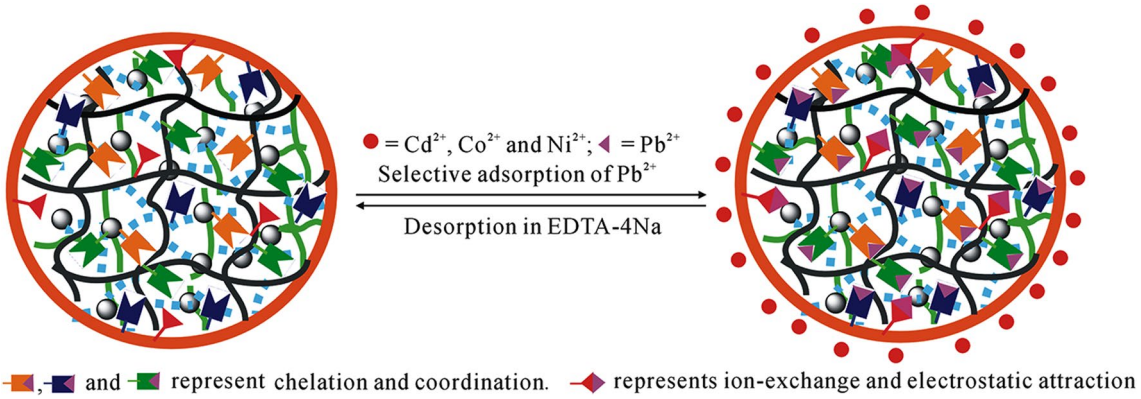

Scheme 2 Possible selective adsorption and desorption mechanism between CS/ATP/PAA hydrogel and Pb^{2+} ions

ATP/PAA hydrogel has been successfully prepared that has a rough and porous network structure. The adsorption results showed that the optimal adsorption pH was 4.8, the time of adsorption equilibrium was 60 min, and the maximum adsorption capacity based on Langmuir isotherm of CS/ATP/PAA absorbent for Pb^{2+} was 531.9 mg g^{-1}. The

adsorption kinetics and adsorption isotherm fitted well to the pseudo-second-order kinetic model and Langmuir isotherm, respectively. The CS/ATP/PAA adsorbent exhibited excellent reusability using EDTA-4Na as eluent and promising selectivity for Pb^{2+} ions with the coexistence of Cd^{2+}, Co^{2+} and Ni^{2+} ions. XPS analysis suggested that the adsorption of CS/ATP/PAA absorbent for Pb^{2+} presented coordination between N or O atoms and Pb^{2+} ions, and ion-exchange between Na^{+} and Pb^{2+}. All results suggested that GDEP can provide a new method for the synthesis of CS/ATP/PAA hydrogel which is a very outstanding absorbent for efficient removal and recovery of Pb^{2+} ions from aqueous solutions.

Acknowledgements This work was supported in part by Natural Science Foundation of Gansu Province (17JR5RA075 and 17JR5RA077), and National Natural Science Foundation of China (Nos. 21567025, 21864022 and 21367023), China.

References

1. Ali I (2012) New generation adsorbents for water treatment. Chem Rev 112:5073–5091
2. Ali I, Peng CS, Lin DC, Saroj DP, Naz I, Khan ZM, Sultan M, Ali M (2019) Encapsulated green magnetic nanoparticles for the removal of toxic Pb^{2+} and Cd^{2+} from water: development, characterization and application. J Environ Manag 234:273–289
3. Khazaei M, Nasseri S, Ganjali MR, Khoobi M, Nabizadeh R, Gholibegloo E, Nazmara S (2018) Selective removal of lead ions from aqueous solutions using 1,8-dihydroxyanthraquinone (DHAQ) functionalized graphene oxide: isotherm, kinetic and thermodynamic studies. RSC Adv 8:5685–5694
4. Wang NN, Xu XJ, Li HY, Zhai JL, Yuan LZ, Zhang KX, Yu HW (2016) Preparation and application of a xanthate-modified thiourea chitosan sponge for the removal of Pb(II) from aqueous solutions. Ind Eng Chem Res 55:4960–4968
5. Liu YM, Ju XJ, Xin Y, Zheng WC, Wang W, Wei J, Xie R, Liu Z, Chu LY (2014) A novel smart microsphere with magnetic core and ion-recognizable shell for Pb^{2+} adsorption and separation. ACS Appl Mater Interfaces 6:9530–9542
6. Liu B, Lv X, Meng X, Yu G, Wang D (2013) Removal of Pb(II) from aqueous solution using dithiocarbamate modified chitosan beads with Pb(II) as imprinted ions. Chem Eng J 220:412–419
7. World Health Organisation (2011) Guidelines for drinking-water quality, 4th ed, Geneva, 383–384.
8. Yu J, Zheng JD, Lu QF, Yang SX, Zhang XM, Wang X, Yang W (2016) Selective adsorption and reusability behavior for Pb^{2+} and Cd^{2+} on chitosan/poly(ethylene glycol)/poly(acrylic acid) adsorbent prepared by glow-discharge electrolysis plasma. Colloid Polym Sci 294:1585–1598
9. Akkaya R, Ulusoy U (2008) Adsorptive features of chitosan entrapped in polyacrylamide hydrogel for Pb^{2+}, UO_2^{2+}, and Th^{4+}. J Hazard Mater 151:380–388
10. Li Z, Xiao D, Ge Y, Koehler S (2015) Surface-functionalized porous lignin for fast and efficient lead removal from aqueous solution. ACS Appl Mater Interf 7:15000–15009
11. Fan QH, Li Z, Zhao HG, Jia ZH, Xu JZ, Wu WS (2009) Adsorption of Pb(II) on palygorskite from aqueous solution: effects of pH, ionic strength and temperature. Appl Clay Sci 45:111–116
12. Wang S, Ariyanto E (2007) Competitive adsorption of malachite green and Pb ions on natural zeolite. J Colloid Interf Science 314:25–31
13. Lu QF, Yu J, Gao JZ, Yang W, Li Y (2011) Glow-discharge electrolysis plasma induced synthesis of polyvinylpyrrolidone/acrylic acid hydrogel and its adsorption properties for heavy-metal ions. Plasma Process Polym 8:803–814
14. Yu J, Zhang HT, Li Y, Lu QF, Wang QZ, Yang W (2016) Synthesis, characterization, and property testing of PGS/P(AMPS-co-AM) superabsorbent hydrogel initiated by glow-discharge electrolysis plasma. Colloid Polym Sci 294:257–270
15. Yu J, Zheng JD, Lu QF, Yang SX, Wang X, Zhang XM, Yang W (2016) Reusability and selective adsorption of Pb^{2+} on chitosan/P(2-acryl amido-2-methyl-1-propanesulfonic acid-co-acrylic acid) hydrogel. Iran Polym J 25:1009–1019
16. Gao JZ, Ma DL, Lu QF, Li Y, Li XF, Yang W (2010) Synthesis and characterization of montmorillonite-graft-acrylic acid superabsorbent by using glow-discharge electrolysis plasma. Plasma Chem Plasma Process 30:873–883
17. Liu P, Jiang L, Zhu L, Wang A (2014) Novel approach for attapulgite/poly(acrylic acid) (ATP/PAA) nanocomposite microgels as selective adsorbent for Pb(II) ion. React Funct Polym 74:72–80
18. Deng Y, Gao Z, Liu B, Hu X, Wei Z, Sun C (2013) Selective removal of lead from aqueous solutions by ethylenediamine-modified attapulgite. Chem Eng J 223:91–98
19. Liu Y, Zheng Y, Wang AQ (2010) Enhanced adsorption of methylene blue from aqueous solution by chitosan-g-poly(acrylic acid)/vermiculite hydrogel composites. J Environ Sci-China 22:486–493
20. Yu J, Li Y, Lu QF, Zheng JD, Yang SX, Jin F, Wang QZ, Yang W (2016) Synthesis, characterization and adsorption of cationic dyes by CS/P(AMPS-co-AM) hydrogel initiated by glow-discharge electrolysis plasma. Iran Polym J 25:423–435
21. Vakili M, Deng SB, Li T, Wang W, Wang WJ, Yu G (2018) Novel crosslinked chitosan for enhanced adsorption of hexavalent chromium in acidic solution. Chem Eng J 347:782–790
22. Aliabadi M, Irani M, Ismaeili J, Piri H, Parnian MJ (2013) Electrospun nanofiber membrane of PEO/chitosan for the adsorption of nickel, cadmium, lead and copper ions from aqueous solution. Chem Eng J 220:237–243
23. Ge H, Hua T, Chen X (2016) Selective adsorption of lead on grafted and crosslinked chitosan nanoparticles prepared by using Pb^{2+} as template. J Hazard Mater 308:225–232
24. Gad YH (2008) Preparation and characterization of poly(2-acrylamido-2- methylpropane-sulfonic acid)/chitosan hydrogel using gamma irradiation and its application in wastewater treatment. Radiat Phys Chem 77:1101–1107
25. Nguyen NT, Liu JH (2013) Fabrication and characterization of poly(vinyl alcohol)/chitosan hydrogel thin films via UV-irradiation. Eur Polym J 49:4201–4211
26. Yu J, Yang GG, Pan YP, Lu QF, Yang W, Gao JZ (2014) Poly (acrylamide-co-acrylic acid) hydrogel induced by glow-discharge electrolysis plasma and its adsorption properties for cationic dyes. Plasma Sci Technol 16:767–776
27. Zou LZ, Shao PH, Zhang K, Yang LM, You D, Shi H, Pavlostathis SG, Lai WQ, Liang DH, Lou XB (2019) Tannic acid-based adsorbent with superior selectivity for lead(II) capture: adsorption site and selective mechanism. Chem Eng J 364:160–166
28. Yu J, Zhang XM, Lu QF, Sun DX, Wang X, Zhu SW, Zhang ZC, Yang W (2018) Evaluation of analytical performance for the simultaneous detection of trace Cu, Co and Ni by using liquid cathode glow discharge-atomic emission spectrometry. Spectrochim Acta B 145:64–70
29. Lu QF, Yang SX, Sun DX, Zheng JD, Li Y, Yu J, Su MG (2016) Direct determination of Cu by liquid cathode glow discharge-atomic emission spectrometry. Spectrochim Acta B 125:136–139

30. Liu Y, Sun B, Wang L, Wang D (2012) Characteristics of light emission and radicals formed by contact glow discharge electrolysis of an aqueous solution. Plasma Chem Plasma Process 32:359–368
31. Hsieh KC, Wang H, Locke BR (2016) Analysis of electrical discharge plasma in a gas-liquid flow reactor using optical emission spectroscopy and the formation of hydrogen peroxide. Plasma Process Polym 13:908–917
32. Joshi RP, Thagard SM (2013) Streamer-like electrical discharges in water: part II. Environmental applications. Plasma Chem Plasma Process 33:17–49
33. Brisset JL, Moussa D, Doubla A, Hnatiuc E, Hnatiuc B, Youbi GK, Herry JM, Naïtali M, Bellon-Fontaine MN (2008) Chemical reactivity of discharges and temporal post-discharges in plasma treatment of aqueous media: examples of gliding discharge treated solutions. Ind Eng Chem Res 47:5761–5781
34. Huang J, Liu Y, Jin Q, Wang X, Yang J (2007) Adsorption studies of a water soluble dye, Reactive Red MF-3B, using sonication-surfactant-modified attapulgite clay. J Hazard Mater 143:541–548
35. Fan QH, Shao DD, Hu J, Wu WS, Wang XK (2008) Comparison of Ni^{2+} sorption to bare and ACT-graft attapulgites: effect of pH, temperature and foreign ions. Surf Sci 602:778–785
36. Liu J, Wang Q, Wang A (2007) Synthesis and characterization of chitosan-g-poly(acrylic acid)/sodium humate superabsorbent. Carbohyd Polym 70:166–173
37. Zhao F, Repo E, Sillanpää M, Meng Y, Yin D, Tang WZ (2015) Green synthesis of magnetic EDTA- and/or DTPA-cross-linked chitosan adsorbents for highly efficient removal of metals. Ind Eng Chem Res 54:1271–1281
38. Ren Y, Abbood HA, He F, Peng H, Huang K (2013) Magnetic EDTA-modified chitosan/SiO_2/Fe_3O_4 adsorbent: preparation, characterization, and application in heavy metal adsorption. Chem Eng J 226:300–311
39. Benamer S, Mahlous M, Tahtat D, Nacer-Khodja A, Arabi M, Lounici H, Mameri N (2011) Radiation synthesis of chitosan beads grafted with acrylic acid for metal ions sorption. Radiat Phys Chem 80:1391–1397
40. Vasconcelos HL, Guibal E, Laus R, Vitali L, Fávere VT (2009) Competitive adsorption of Cu(II) and Cd(II) ions on spray-dried chitosan loaded with Reactive Orange 16. Mater Sci Eng C 29:613–618
41. Manasi Rajesh V, Rajesh N (2015) An indigenous *Halomonas BVR1* strain immobilized in crosslinked chitosan for adsorption of lead and cadmium. Int J Biol Macromol 79:300–308
42. Yan H, Dai J, Yang Z, Yang H, Cheng R (2011) Enhanced and selective adsorption of copper(II) ions on surface carboxymethylated chitosan hydrogel beads. Chem Eng J 174:586–594
43. Lu Y, He J, Luo G (2013) An improved synthesis of chitosan bead for Pb(II) adsorption. Chem Eng J 226:271–278
44. Chauhan D, Sankararamakrishnan N (2008) Highly enhanced adsorption for decontamination of lead ions from battery wastewaters using chitosan functionalized with xanthate. Bioresour Technol 99:9021–9024
45. Laus R, Costa TG, Szpoganicz B, Fávere VT (2010) Adsorption and desorption of Cu(II), Cd(II) and Pb(II) ions using chitosan crosslinked with epichlorohydrin-triphosphate as the adsorbent. J Hazard Mater 183:233–241
46. Lyu FY, Yu HQ, Hou TL, Yan LG, Zhang XH, Du B (2019) Efficient and fast removal of Pb^{2+} and Cd^{2+} from an aqueous solution using a chitosan/Mg-Al-layered double hydroxide nanocomposite. J Colloid Interf Sci 539:184–193
47. Zhou D, Zhang L, Guo S (2005) Mechanisms of lead biosorption on cellulose/chitin beads. Water Res 39:3755–3762
48. Chen M, Shafer-Peltier K, Randtke SJ, Peltier E (2018) Competitive association of cations with poly(sodium 4-styrenesulfonate) (PSS) and heavy metal removal from water by PSS-assisted ultrafiltration. Chem Eng J 344:155–164
49. Wan Ngah WS, Fatinathan S (2010) Pb(II) biosorption using chitosan and chitosan derivatives beads: equilibrium, ion exchange and mechanism studies. J Environ Sci 22:338–346
50. Cai H, Sun Y, Zhang X, Zhang L, Liu H, Li Q, Bo TZ, Zhou DZ, Wang C, Lian J (2019) Reduction temperature-dependent nanoscale morphological transformation and electrical conductivity of silicate glass microchannel plate. Materials 12:1183